Molecular origin of the weak susceptibility of kinesin velocity to loads and its relation to the collective behavior of kinesins

Qian Wang[a], Michael R. Diehl[b,c], Biman Jana[d], Margaret S. Cheung[a,e], Anatoly B. Kolomeisky[a,b,c], and José N. Onuchic[a,c,f,g,1]

[a]Center for Theoretical Biological Physics, Rice University, Houston, TX 77005; [b]Department of Bioengineering, Rice University, Houston, TX 77030; [c]Department of Chemistry, Rice University, Houston, TX 77030; [d]Department of Physical Chemistry, Indian Association for the Cultivation of Science, Jadavpur, Kolkata 700032, India; [e]Department of Physics, University of Houston, Houston, TX 77204; [f]Department of Physics and Astronomy, Rice University, Houston, TX 77005; and [g]Department of Biosciences, Rice University, Houston, TX 77005

Contributed by José N. Onuchic, September 2, 2017 (sent for review June 7, 2017; reviewed by Ioan Andricioaei and Garegin A. Papoian)

Motor proteins are active enzymatic molecules that support important cellular processes by transforming chemical energy into mechanical work. Although the structures and chemomechanical cycles of motor proteins have been extensively investigated, the sensitivity of a motor's velocity in response to a force is not well-understood. For kinesin, velocity is weakly influenced by a small to midrange external force (weak susceptibility) but is steeply reduced by a large force. Here, we utilize a structure-based molecular dynamic simulation to study the molecular origin of the weak susceptibility for a single kinesin. We show that the key step in controlling the velocity of a single kinesin under an external force is the ATP release from the microtubule-bound head. Only under large loading forces can the motor head release ATP at a fast rate, which significantly reduces the velocity of kinesin. It underpins the weak susceptibility that the velocity will not change at small to midrange forces. The molecular origin of this velocity reduction is that the neck linker of a kinesin only detaches from the motor head when pulled by a large force. This prompts the ATP binding site to adopt an open state, favoring ATP release and reducing the velocity. Furthermore, we show that two load-bearing kinesins are incapable of equally sharing the load unless they are very close to each other. As a consequence of the weak susceptibility, the trailing kinesin faces the challenge of catching up to the leading one, which accounts for experimentally observed weak cooperativity of kinesins motors.

kinesin | molecular mechanism | susceptibility | collective behavior

Motor proteins or biological molecular motors are active enzymatic molecules that help control the internal organization of cells by driving the movements of vesicles and organelles along cytoskeletal filaments (1, 2). The molecular structures (3–9), chemomechanical cycles (10–12), and regulation mechanisms (13–20) of these critical mechanical enzymes have been studied extensively to resolve how these proteins convert the free energy available from ATP hydrolysis into mechanical motion. A number of precision biophysical techniques have been developed to characterize the motor step sizes, unloaded velocities, stalling forces, and processivity, since these properties are crucial to understand how motors transport their cargo and are often used to distinguish the different classes of motors expressed in cells. However, the slope of single-motor force–velocity relationships (dv/dF), which has also been referred to as the susceptibility of the motor velocity to load, $\chi_{vel}(F)$, has also been shown to be critical to motor mechanics, particularly when motors function collectively. Theoretical analyses showed that $\chi_{vel}(F)$ can be a key determinant of the active contractility in actomyosin networks (21) as well as in the collective force generation by multiple motor proteins overcoming an opposing force in a viscous cellular milieu (22–24). In both cases, $\chi_{vel}(F)$ defines how rapidly a system of coupled motors can adapt its filament-bound configuration to balance the forces between its constituent motors.

$\chi_{vel}(F)$ is a complex parameter that can vary considerably depending on the motor type and across different loading regimes. Previous single-molecule analyses have shown that the kinesin motor velocity changes sluggishly at low loads [i.e., $\chi_{vel}(F)$ is low below the single-kinesin stalling force] (25). In contrast, the velocities of single myosin and dynein motors decrease much more rapidly at low loads, yielding a stronger $\chi_{vel}(F)$ in the same loading regime (26, 27). Herein, we pinpointed the molecular origin of the weak $\chi_{vel}(F)$ for kinesins by analyzing the impact of loading forces on the transition rates in the chemomechanical cycle. Using structure-based molecular dynamics simulations, we identified the ATP release rate as the key reason for the weak susceptibility of kinesin velocity to the small loading forces (Fig. 1*A*). We discovered that the contact formation between the neck linker and the motor head is coupled to the dynamics of the open or the closed state of the ATP binding site through a preserved coevolving network formed by α6, β1/β6, and switch I/II within the motor head. Such coupling is only activated at large loading forces, leading to the weak $\chi_{vel}(F)$ to small loading forces.

Finally, building on this framework, we further examined how the $\chi_{vel}(F)$ of a single kinesin influences the cooperativity of

Significance

Successful functioning of biological systems depends on efficient cellular transport supported by several classes of active biological molecules known as motor proteins. Although they have been intensively studied using various experimental methods, their molecular properties remain not fully understood. We developed a theoretical approach by using structure-based molecular dynamics simulations. It allowed us to understand at the molecular level the effect of external forces on kinesin motor proteins. It is shown that a force-regulated coupling between the neck linker and the ATP binding site of a kinesin accounts for experimentally observed weak susceptibility to loads. Our framework helps us to rationalize the low cooperativity among kinesins. The presented method is a powerful tool in clarifying microscopic features of motor proteins.

Author contributions: Q.W., M.S.C., A.B.K., and J.N.O. designed research; Q.W. performed research; Q.W., M.R.D., B.J., M.S.C., A.B.K., and J.N.O. analyzed data; and Q.W., M.R.D., B.J., M.S.C., A.B.K., and J.N.O. wrote the paper.

Reviewers: I.A., University of California, Irvine; and G.A.P., University of Maryland.

The authors declare no conflict of interest.

[1]To whom correspondence should be addressed. Email: jonuchic@rice.edu.

This article contains supporting information online at www.pnas.org/lookup/suppl/doi:10.1073/pnas.1710328114/-/DCSupplemental.

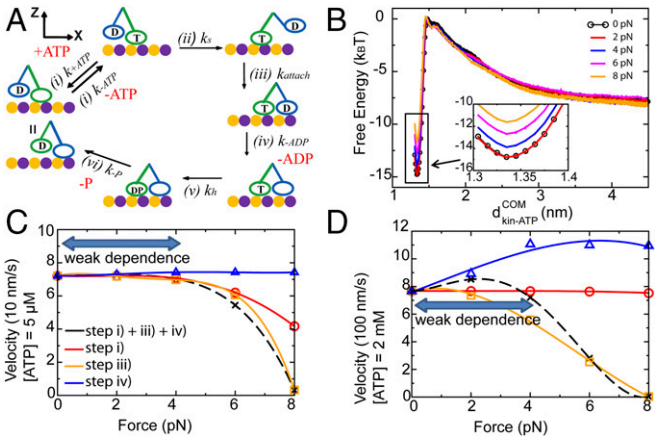

Fig. 1. The chemomechanical cycle of a single double-headed kinesin under an external force. (*A*) A schematic diagram of the chemomechanical cycle of a single double-headed kinesin on an MT. T represents an ATP-bound motor head. D represents an ADP-bound motor head. DP represents an ADP·P-bound motor head; *k* represents the reaction rate of each step in a cycle. (*B*) The free energy profile of binding/unbinding between the ATP and the leading head (LH) in step *i* at 300 K with external loading forces of $F = 0$, 2, 4, 6, and 8 pN separately. $d^{COM}_{kin-ATP}$ represents the distance between the center of mass of ATP and that of the LH. The free energy profile in the bound state ($d^{COM}_{kin-ATP} = 1.34$ nm) is zoomed in and shown in *Inset*. (*C* and *D*) Numerically calculated velocity of single kinesin as a function of external loading forces at (*C*) 5 μM ATP and (*D*) 2 mM ATP. The black dashed lines represent the calculated velocity when steps *i*, *iii*, and *iv* are all force-dependent. The profile shows a weak dependence on small forces. The red solid lines represent the calculation assuming that only step *i* is force-dependent. For other steps, we assume that they are force-independent. The orange solid lines represent the calculation assuming that only step *iii* is force-dependent. The blue solid lines represent the calculation assuming that only step *iv* is force-dependent. Steps *i* (ATP release) and *iii* (attachment) cause a slow decrease in the velocity under loading forces. They serve as important steps to resist small forces. Error bars are shown in *B*.

multiple kinesin proteins. To this end, we developed a quantitative relationship between the force partitioning and the spatial arrangement between two kinesins on their filament using an atomistic structure of kinesins docking on the microtubule (MT) and molecular dynamic simulations. The force partitioning can be directly measured from our ab initio simulations. We found that the leading kinesin takes more than 90% of the overall load when the distance between two kinesins is larger than 48 nm. With the weak susceptibility, $\chi_{vel}(F)$, it is difficult for the trailing kinesin to catch up with the leading one. Therefore, the uneven force partitioning remains and leads to the low cooperativity between two kinesins. Our study provides a structural basis of $\chi_{vel}(F)$, which is critical to fully understand the collective behavior of multiple motors and facilitate potential protein engineering for high-efficiency motors.

Results and Discussion

Determine the Key Chemical Steps That Account for the Weak Susceptibility of Kinesin Velocity to External Loads. Experimental studies show that the overall velocity of a kinesin slowly decreases under loading forces unless the forces approach the stalling force (25). We interrogated the impact of loading forces on the reaction rate for each chemical step of the chemomechanical cycle (Fig. 1*A*) to identify the key chemical steps that account for weak susceptibility of kinesin velocity to external loads, $\chi_{vel}(F)$. The chemomechanical cycle starts from a process when the leading head of a kinesin on a MT binds an ATP, while the ADP-bound trailing head detaches from the MT (Fig. 1*A*, step *i*). In the next chemical step, the ADP-bound trailing head swings from the back to the front of the ATP-bound leading head (Fig. 1*A*, step *ii*). The new ADP-bound leading head steps on the MT (Fig. 1*A*, step *iii*) and releases ADP (Fig. 1*A*, step *iv*). Finally, the cycle ends with the hydrolysis of ATP at the ATP-bound trailing head followed by the release of phosphate (Fig. 1*A*, steps *v* and *vi*). The structures of kinesins are known for steps *i*, *iii*, and *iv* in particular, which allows us to evaluate the changes in the free energy landscape under force by means of molecular dynamics simulations. The velocity of a single kinesin can be calculated from the simplified Michaelis–Menten framework presented below in Eqs. **1**–**3** (details of derivations are in *Michaelis–Menten Representation of the Kinesin Cycle*):

$$V = \delta \frac{k^{eff}_{cat}[S]}{K^{eff}_M + [S]} \quad [1]$$

$$k^{eff}_{cat} = \left(\frac{1}{k_s} + \frac{1}{k_{attach}} + \frac{1}{k_{-ADP}} + \frac{1}{k_h} + \frac{1}{k_{-p}}\right)^{-1} \quad [2]$$

$$K^{eff}_M = \frac{k^{eff}_{cat}}{k_s}\left(\frac{k_s + k_{-ATP}}{k_{+ATP}}\right). \quad [3]$$

k_{ATP}, k_{-ATP}, k_s, k_{attach}, k_{-ADP}, k_h, and k_{-p} are the rates of the chemical reaction for the key steps in Fig. 1*A*. $[S]$ is the concentration of ATP. δ is the step size of kinesin: 8 nm.

In the following, utilizing high-resolution structures of kinesin obtained in previous experiments (3, 4), we created a structure-based coarse-grained model to derive the free energy surfaces along chosen reaction coordinates for several chemical steps in the chemomechanical cycle of a single kinesin (steps *i*, *iii*, and *iv* in Fig. 1*A*). Those free energy surfaces were found to be modulated by external forces differently. Next, the kinetic rates as a function of external forces were calculated from the free energy surfaces. In this way, we were able to determine the key chemical steps in the cycle that account for the low $\chi_{vel}(F)$ of a single kinesin. As detailed below, those chemical steps are ATP release (step *i*) and attachment (step *iii*) (Fig. 1*A*). We will further explain the relationship of $\chi_{vel}(F)$ that characterizes the gait of a single kinesin and the cooperativity between two kinesins in later sections.

Step i. The reaction coordinate was chosen to be the distance between the center of mass of ATP and that of the leading head of the kinesin, $d^{COM}_{kin-ATP}$ (Fig. 1*B*). The free energy barrier of ATP release is defined by the free energy between the ATP-bound state ($d^{COM}_{kin-ATP} = 1.34$ nm) and the transition state ($d^{COM}_{kin-ATP} = 1.46$ nm), ΔG_r. We found that the difference between ΔG_r at $F = 2$ pN and that at $F = 0$ is less than 0.1 k_BT, indicating that ATP release is barely affected by a small loading force. ΔG_r slowly increases with loading force. At a large force of 8 pN, ΔG_r decreases by 3 k_BT compared with the case at $F = 0$, indicating a significant increase in the rate of ATP release under large external loading forces. Based on Eqs. **1** and **3**, an increase in the rate of ATP release decreases the velocity of a single kinesin. The negligible change in ΔG_r at 2 pN as well as the slow increase in ΔG_r from 2 to 8 pN imply a weak $\chi_{vel}(F)$ at small loading forces.

Step iii. The reaction coordinate was chosen to be the distance between the center of mass of the leading head and that of the MT along the normal to the MT at $F = 0$ pN and $F = 8$ pN (Fig. S1). The free energy barrier of attachment increases at $F = 8$ pN compared with that at $F = 0$. This increase corresponds to a lowered attaching rate under loading forces and thus, contributes to the smaller velocity of kinesin from Eqs. **1**–**3**.

Step iv. The reaction coordinate was chosen to be the distance between the center of mass of ADP and that of the leading head of the kinesin, $d^{COM}_{kin-ADP}$ (Fig. S2). Under an external loading force

of 8 pN, the free energy barrier of ADP release decreases. The overall velocity of a kinesin grows with an increase in the rate of ADP release under an external loading force.

We examined whether our model could reproduce the weak χ_{vel} *(F)* observed in the experiment (25) at small loading forces. The rate of a certain chemical step can be calculated by the mean first passage time method (28) (details are in *Calculate the Force–Velocity Curve from Simulation Data*) by Eqs. **4** and **5**:

$$k(F)=\left(\int_{X_0}^{X_1} dX \int_{0}^{X} \frac{dX' e^{\frac{G(X,F)-G(X',F)}{k_B T}}}{D(X)}\right)^{-1} \quad [4]$$

$$D(X)=\frac{1}{2}\frac{d\langle X^2\rangle}{dt}. \quad [5]$$

X is the reaction coordinate. D is the diffusion coefficient along the reaction coordinate. G *(X, F)* is the free energy under an external loading force F. Steps *i*, *iii*, and *iv* are all force-dependent chemical steps (Fig. 1*B* and Figs. S1 and S2). The velocity of a single kinesin under external loading forces can be calculated by substituting the rates of those steps obtained in Eqs. **4** and **5** to the expression of the velocity in Eqs. **1**–**3** at both a low concentration (5 μM) (black curve in Fig. 1*C*) and a high concentration (2 mM) (black curve in Fig. 1*D*) of ATP. The predicted velocities reproduce the weak χ_{vel} *(F)* at small loading forces observed in the experiment (25), indicating that our model qualitatively captures the unique response of a single kinesin to external loading forces, despite neglecting the force dependence in steps *ii*, *v*, and *vi*. Step *ii* was not investigated, because it was shown experimentally (29) that the stepping of an ADP-bound trailing head is on the order of several microseconds under F = 5 pN, whereas the other steps in the chemomechanical cycle are of the order of milliseconds (30). Thus, the time spent in step *ii* is too short to influence the velocity of a single kinesin at moderate loading forces. Although backward stepping is a possibility at a large force of 8 pN (29), accounting for this possibility is beyond the scope of our study. Steps *v* and *vi* were also neglected. Without the crystal structure for a kinesin with both ADP and phosphate, it is difficult to realistically apply our structure-based model for these steps. We assumed that these steps are less affected by external loading forces. As mentioned above, even with this approximation, we can still qualitatively reproduce the weak χ_{vel} *(F)* from simulation data. The details of these two steps will be investigated in future works. For Fig. 1*D*, there is a slight increase in the kinesin velocity from 767 nm/s at $F = 0$ to 852 nm/s at $F = 2$ pN. This is because the increase in velocity from step *iv* is slightly larger than the decrease of velocity from other steps at a lower force according to our simulations. This minor increase is small in comparison with the overall changes of the velocity in Fig. 1*D*. Thus, this slight increase does not influence the main conclusion of this work.

To dictate the key chemical steps accounting for the weak χ_{vel} *(F)*, we decomposed the overall response to loading forces into three individual steps. The velocity was recalculated by assuming that only step *i* is force-dependent (red curves in Fig. 1 *C* and *D*), that only step *iii* is force-dependent (orange curves in Fig. 1 *C* and *D*), or that only step *iv* is force-dependent (blue curves in Fig. 1 *C* and *D*). The results indicate that both steps *i* and *iii* lead to a slow decrease in the velocity of a single kinesin under external loading forces, while step *iv* causes an increase in the velocity. We concluded that steps *i* (ATP release) and *iii* (attachment) are the key steps that determine the weak χ_{vel} *(F)* for a single kinesin. At a low concentration of ATP, step *iv* (ADP release) does not affect the velocity of kinesin (Fig. 1*C*, blue line). However, at a high concentration of ATP, step *iv* might be important to maintain the overall velocity of kinesin, because it counteracts the impact from other steps (Fig. 1*D*, blue line). In the next section, we will discuss the molecular origin of these observations.

Molecular Origin of the Weak Susceptibility of Kinesin Velocity to External Loads. It is easy to understand why step *iii* does not introduce a sensitive response of the velocity of a single kinesin to external loading forces. In the absence of forces, the attachment rate constant is 11 $\mu M^{-1}\,s^{-1}$ (11). For a single head-bound state, the effective MT concentration can be ∼1 mM (11), which leads to an attachment rate of 11,000 s^{-1}. This value is orders of magnitude faster than other steps. As a result, the velocity is much less affected by this step unless the force is sufficiently large to decrease the rate of this step, such that it is comparable with that of other steps. Fig. 1 *C* and *D* shows that, only when $F >$ 4 pN (the rate decreases to 264 s^{-1}), this step begins to influence the velocity of kinesin.

For step *i*, it can be argued that, at high concentrations of ATP, when the ATP binding rate is much faster than the ATP release rate, the weak χ_{vel} *(F)* might be caused by the fact that external loading forces largely affect the ATP release rate rather than the ATP binding rate as shown in Fig. 1*B*. Nevertheless, experiments show that this weak χ_{vel} *(F)* exists at both high (2 mM) and low (5 μM) concentrations of ATP (25). It is reasonable to speculate that such a weak χ_{vel} *(F)* also comes from structural changes in the kinesin molecule itself.

We note that the fraction of native contact formations between ATP and kinesin in its ATP-bound state (Q_I; Q_I ranges from zero to one) is a useful parameter to distinguish key conformations in response to ATP release under forces. Below, we relate the impact of forces exerted on the neck linker at one side of the motor head to the opposite side, where it releases ATP in two steps. First, we plotted a 2D potential of mean force (PMF) as a function of the radius of gyration (R_g) of the ATP binding pocket and Q_I (Fig. 2 *A*–*E*). The ATP binding pocket includes kinesin residues within 10 Å of the ATP surface (shown in Fig. S3). At $F = 0$ pN (Fig. 2*A*) and $F = 2$ pN (Fig. 2*B*), the closed state dominantly populates at R_g = 9.4 Å and Q_I = 0.8. At F = 8 pN, the open state is mostly populated at R_g = 10.2 Å and Q_I = 0.1 (Fig. 2*E*). The presence of a large force favors a structurally open state of the ATP binding pocket, which weakens the contacts between ATP and the motor head.

Second, we plotted the PMF as a function of the R_g of the ATP binding pocket and the fraction of native contact formation between the neck linker and motor head, Q_L (ranging from zero to one; $Q_L = 1$ is when the neck linker completely binds to the motor head). In the absence of loading forces (Fig. 2*F*), the dominant basin is Q_L = 0.7, and R_g = 9.4 Å (closed state), indicating that the contact formation between the neck linker and the motor head of a single kinesin noncompetitively inhibits the ATP release by favoring the closed state of the motor head. It is in accordance with an experimental study showing that both the neck linker and ATP bind to a motor head (31). This coupling between the neck linker and the ATP binding site was also observed by other research groups (32, 33). In this work, we further identified how this coupling was regulated by external loading forces. At a small force of 2 pN (Fig. 2*G*), the dominant basin is the same as that at $F = 0$, indicating that a small force is insufficient to initiate the structural changes that propagate from the neck linker to the ATP binding site. At a large force of 8 pN (Fig. 2*J*), Q_L peaks at 0.1, and R_g reaches an open state of 10.2 Å that favors the release of ATP, indicating that the detachment of the neck linker from motor head could lead to a switch from the "closed" to the "open" state.

Such structural coupling between the neck linker and the ATP binding pocket prompted us to investigate the allosteric intramolecular network. Direct coupling analysis (34) (DCA), a

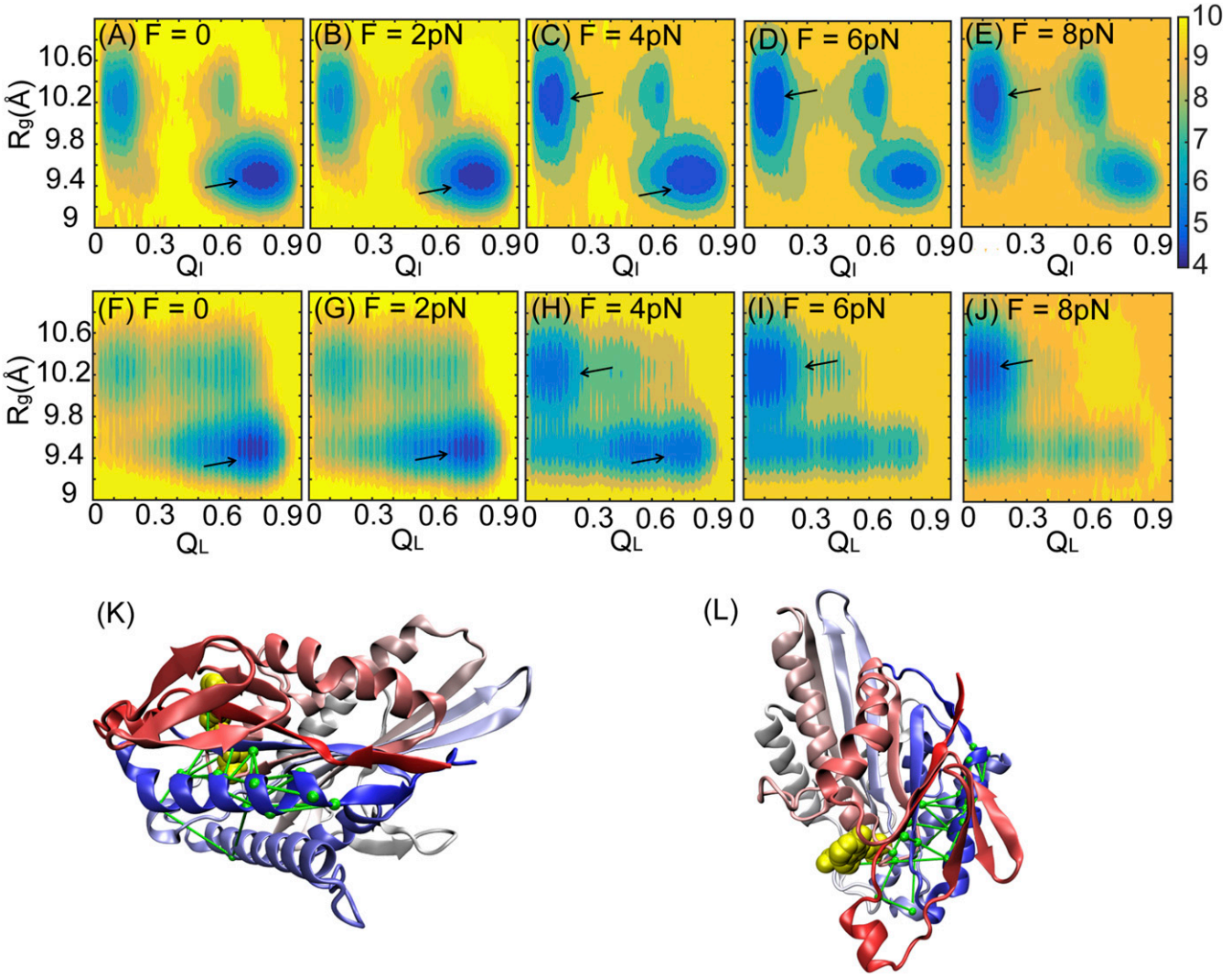

Fig. 2. Conformational changes of a single double-headed kinesin under an external force. (*A*–*E*) 2D free energy as a function of the radius of gyration of the ATP binding pocket, R_g, and the fraction of native contact formation between a single kinesin and ATP, Q_I, at loading forces of $F = 0$, 2, 4, 6, and 8 pN separately. (*F*–*J*) 2D free energy as a function of R_g and the fraction of native contact formation between the leading head and the connecting neck linker, Q_L, at loading forces of $F = 0$, 2, 4, 6, and 8 pN separately. The free energy is colored in units of k_BT at $T = 300$ K. Black arrows point to the basin of the low free energy from each panel. (*K* and *L*) Structure of a motor head and its connecting neck linker with a network of lines from the DCA. The kinesin motor head is colored from red (N terminus) to blue (C terminus) and shown from the front view (*K*) and the top view (*L*). ATP is colored in yellow.

statistical inference framework used to infer direct coevolutionary couplings among residue pairs in multiple sequence alignments, was applied to probe a network of highly coevolutionary tendencies beginning from the neck linker to the ATP binding site. We identified the network through α6, β1/β6, and switch I/II, as shown by green lines in Fig. 2 *K* and *L*. This DCA generalizes the correlated motion that is possibly preserved throughout evolution across the kinesin family.

This intramolecular allostery also exists for the ADP release process, thus explaining the increase in the rate of ADP release, as shown in Fig. S2. In addition, our finding provides a plausible molecular explanation for experimental observations (35), showing that ADP release is controlled by the direction of the loading force. When the direction of the force is opposite to the motion of kinesin, ADP release is favored, because the force disrupts the contact formation between the neck linker and the motor head. When the loading force and kinesin motion are in the same direction, ADP release is hindered, because the attachment of the neck linker to the motor head is favored. Our results seem to disagree with another experimental investigation (36) claiming that external loading forces decrease the rate of ADP release. We noted that the step of ADP release in their kinetic model is equivalent to the combined process of steps *iii* and *iv* in our study. Given that the velocity of a kinesin can either decrease in step *iii* or increase in step *iv* under external force, it is possible that the velocity decreases under force when both steps *iii* and *iv* are considered in our model.

The contact formation between the neck linker and the motor head, which inhibits ATP release, was identified to account for such a weak χ_{vel} *(F)* to small forces. However, because the position of a disordered neck linker (36) with respect to the motor head is not known, one may speculate about the robustness of our major result. To test this hypothesis, we placed the disordered neck linker outside the N terminus of the motor head (Fig. S4*A*). We ran another simulation with a different position of the neck linker by placing it between the N terminus and the main body of a motor head (Fig. S4*B*), which was the arrangement in a previous computational study (13). We found that, under an

external loading force, the structure of the motor head switches from the "closed state" to the "open state," regardless of the relative position of the disordered neck linker with respect to the motor head. In addition, we calculated the structural differences between the closed and open states for both cases (neck linker is "inside" in Fig. S5*A*, and neck linker is "outside" in Fig. S5*B*). The findings in Fig. S5 *A* and *B* are very similar (Fig. S5*C*). Therefore, it can be concluded that our results do not depend on the position of the neck linker.

Geometric Constraints Cause Uneven Force Partitioning Between Two Load-Bearing Kinesins. We further examined how the weak susceptibility of kinesin velocity to external loads, $\chi_{vel}(F)$, influences the cooperativity of multiple kinesin proteins. The influence was examined by first analyzing the load balancing between two kinesins from coarse-grained molecular simulations (details are in *Coarse-Grained Model and Hamiltonian*). A previous well-known analytical model on the cooperativity of multiple motors was developed by Lipowsky and coworkers (37, 38). Using a mean-field assumption, it was suggested that every motor protein equally shares the loading force from a cargo, implying that the performance of motors grows with the number of motors. However, this mean-field view was challenged by several recent experiments (22–24), which found that two interacting kinesins produce a force much less than expected for a cooperative team.

We applied an external force F on the cargo in the $-X$ direction (Fig. 3*A*) and found that the partitioned force on the leading kinesin under F, $F(LK)/F$, grows with the separation between the two kinesins, D (Fig. 3*B*). As the distance D approaches 48 nm, the leading kinesin shoulders almost the entire external loading force, such that the performance of the two kinesins is essentially represented by one kinesin.

At an external loading force of 8 pN, $F(LK)/F$ reaches 0.9 at $D = 48$ nm, implying that the leading kinesin takes up to 7.2 pN by itself. This force is close to the experimentally measured detaching force of 6–8 pN for a single kinesin (23). This finding is probably the main reason why the detaching force of two kinesins is similar to that of one kinesin according to recent experimental measurements (23). Our coarse-grained model allows the elastic deformation of a kinesin under external forces. Because of such deformation, $F(LK)/F$ at an external load force of 2 pN is 15% greater than that at an external force of 8 pN (Fig. 3*B*), indicating that the cooperativity of two kinesins at $F = 8$ pN is greater than that at $F = 2$ pN. This finding agrees with the experimental observation that the cooperativity of kinesins grows with loading force (22).

This uneven partitioning of forces on the two kinesins was illustrated by a simple geometric constraint (details are explained in *Numerical Calculations on the Force Partitioning of Two Load-Bearing Kinesins*). The distance between a cargo and each of the two kinesins was modeled to follow a simple Hook's law. The leading kinesin is farther from the center of the cargo than the trailing kinesin. Numerically, the outcome that $F(LK)/F$ differs by the loading forces (Fig. S6*A*) agrees with our simulations (Fig. 3*B*). $F(LK)/F$ grows with the stiffness of a motor protein (Fig. S6*B*) and inversely grows with the size of the cargo (Fig. S6*C*). Both calculations agree with other theoretical investigations of the cooperativity of kinesin motor proteins (24, 39).

The Weak Susceptibility of Kinesin Velocity to External Loads Affects the Cooperativity with Another Motor Protein. Because of the geometrical constraints, the partitioning of forces between two load-bearing motors depends on their separation (D). For example, the leading kinesin shares the most load at $D = 48$ nm. The two kinesins share a rather balanced load at $D = 24$ nm, implying better cooperativity than in the former condition (Fig. 3*B*). Thus, the relative movement between the two motors under an external loading force, which determines their separation, becomes the key factor that dictates the cooperativity between two motors. Before we discuss the cooperation between any two interacting motors, we must quantify the relation of their separation D under external loading forces from the force–velocity profile of a single motor.

A motor protein's velocity decreases with external force (25–27) as illustrated in Fig. 4*A*. There are two types of curves that characterize the gait of a single motor under external forces. For a motor protein with a weak $\chi_{vel}(F)$, such as kinesins, the gait follows the upper curve (black in Fig. 4*A*), such that the velocity changes slowly at small forces, as shown in experiments (25). In contrast, for other motor proteins with a strong $\chi_{vel}(F)$, such as myosins and dyneins, the velocity sharply diminishes at low external loads (26, 27), following the lower curve (red in Fig. 4*A*). Because this work only focuses on kinesin, we used the computed force–velocity curve of kinesin (black in Fig. 1*D*) to represent the weak $\chi_{vel}(F)$ (black in Fig. 4*A*) and used an illustrative curve to represent the strong $\chi_{vel}(F)$ (red in Fig. 4*A*).

Given that each forward step of 8 nm for a motor protein occurs in milliseconds, it is prohibitive for us to perform structure-based molecular dynamic simulations on the head-over-head motion of two motor heads. Thus, we modeled a static optical trap experiment and computed D as a function of F by combining computer simulations and numerical calculations, as shown in Fig. 4*B* (details of the method are in *Numerical*

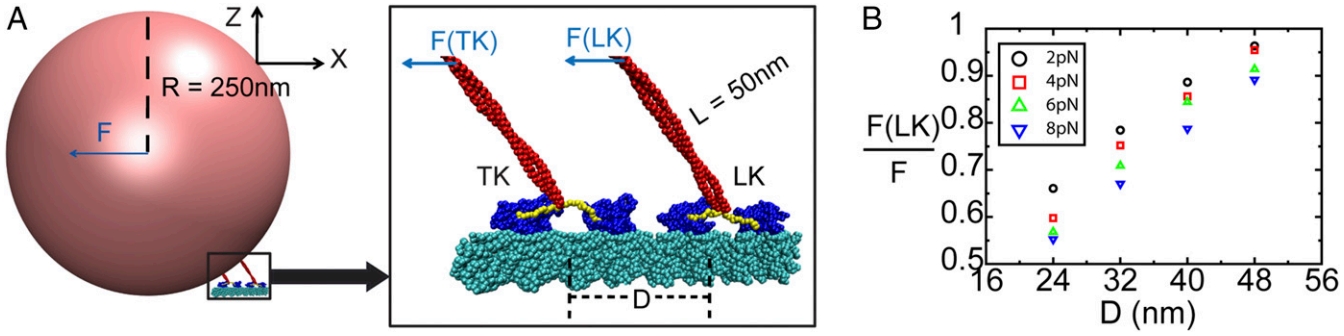

Fig. 3. Force partitioning between two load-bearing kinesins. (*A*) Illustration of two load-bearing kinesins attaching to an MT and jointly carrying a cargo with a radius of 250 nm. The stalk length of each kinesin is 50 nm. The cargo is pulled by an external force in the $-X$ direction. *Right* is the zoomed structure of two kinesins and the MT. The MT is colored cyan. The cargo is colored pink. The motor heads are colored blue. The neck linkers are colored yellow. The stalks are colored red. The separation between two kinesins is D. The external force F is partitioned between the leading kinesin, $F(LK)$, and the trailing kinesin, $F(TK)$. (*B*) Result of the force partitioning, $F(LK)/F$, plotted against D at varying external forces from coarse-grained molecular simulations. This graph shows that the leading kinesin takes the majority of the overall loading forces.

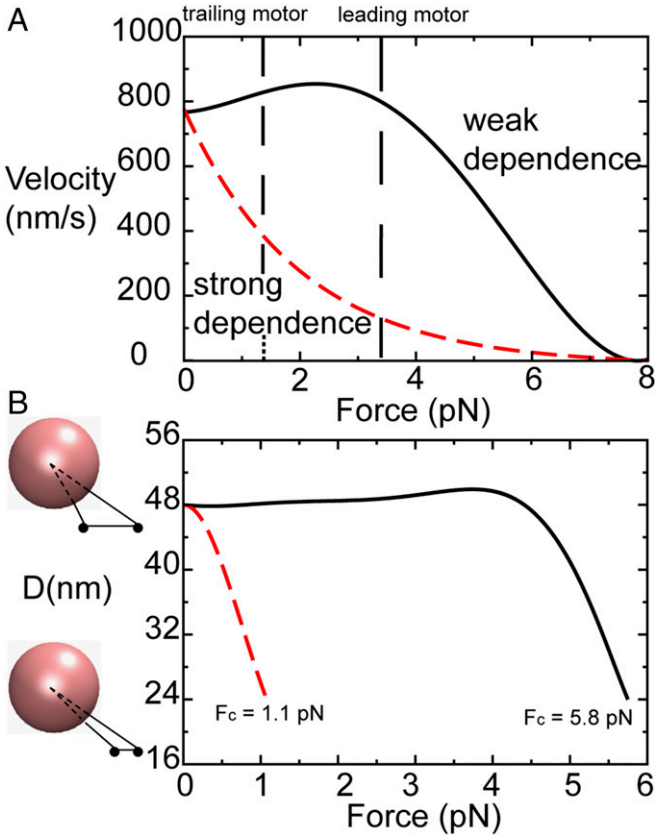

Fig. 4. Numerical calculations on the distance between two load-bearing motor proteins as a function of loading force. (*A*) Two force–velocity relationships for motor proteins. The black solid curve is the numerically calculated force–velocity relationship for a single kinesin, as shown in Fig. 1*D*. This relationship represents the weak susceptibility of kinesin velocity to external loads. In contrast, the red dashed line shows a strong susceptibility. The vertical dashed lines correspond to the forces and velocities experienced by the leading motor and trailing motor in a two-motor load-sharing system. (*B*) Distance between two load-bearing motor proteins, *D*, as a function of the external loading force, *F*, calculated from the curves in *A*, with the computing procedure given in *Numerical Calculations on the Distance Between Two Load-Bearing Motor Proteins as a Function of Loading Force*. F_c denotes the total force on the two interacting kinesins in a triangular configuration when the two are at the smallest separation on an MT, reaching a possibly highest cooperativity. For the black curve (weak susceptibility), F_c is 5.8 pN. For the red curve (strong susceptibility), F_c is 1.1 pN.

Calculations on the Distance Between Two Load-Bearing Motor Proteins as a Function of Loading Force). We denote F_c as the total force on the two interacting kinesins in a triangular configuration when the two are the closest on an MT at $D = 24$ nm, reaching a possibly highest cooperativity. We showed that, for motor proteins that follow the "upper curve" in the force–velocity relationship (Fig. 4*A*, black), F_c is 5.8 pN. In contrast, for motor proteins that follow the "lower curve" in the force–velocity relationship (Fig. 4*A*, red curve), F_c is 1.1 pN. One can ask about the role of F_c for a single motor in the cooperativity between two motors. Since the detachment rate of the motors from the MT increases exponentially with external forces, a high F_c indicates a high probability for the leading motor to detach from the MT before the trailing kinesin catches up with the leading motor; the cooperativity between two motors is low. For the motors that follow the lower curve in the force–velocity profile, their motion is highly cooperative as shown for myosins (40) and dyneins (27) in previous experimental studies.

Our model is able to explain the recent experimental observations in the system of two kinesins carrying a cargo that primarily uses one kinesin for transportation (23). From a structural perspective, we provide snapshots of an intramolecular allostery between the neck linker and the ATP binding pocket of a single kinesin mediated by forces that dictates the weak $\chi_{vel}(F)$ to small forces (Fig. 5, black curve). We can test the validity of our predictions by suggesting a structural mutation on the interface between the neck linker and the motor head that would allow a kinesin to follow the lower curve in Fig. 5 (red curve). We would expect an increase in cooperativity between two interacting mutant kinesins.

The biological importance of $\chi_{vel}(F)$ was further manifested in a group of collaborating protein motors. In bidirectional transportation with frequent reversals (41, 42), kinesins and dyneins moving in opposite directions are required to jointly drive a cargo (38, 43). When there are multiple copies of dyneins against multiple copies of kinesins, the odds of winning for dyneins grow when they work in teams. The distinctive gait of a motor protein with varying force–velocity dependence facilitates frequent reversals of the moving direction when they work in teams (41, 42).

Conclusion

We delineate the weak susceptibility of kinesin velocity to external loads by showing that only under large loading forces can the motor head release ATP at a fast rate; thus, the velocity of kinesin significantly reduces. The molecular origin of the weak susceptibility is the intramolecular coupling between the neck linker and ATP binding site of kinesin, which only activates under large forces. This coupling is preserved by a network of coevolving amino acids that form α6, β1/β6, and switch I/II within the motor head. For two load-bearing kinesins, the leading kinesin takes more than 90% of an overall load when their separation is larger than 48 nm. Because of the weak susceptibility, it is unfavorable for the trailing kinesin to catch up with the leading one, contributing a low cooperativity between two kinesins.

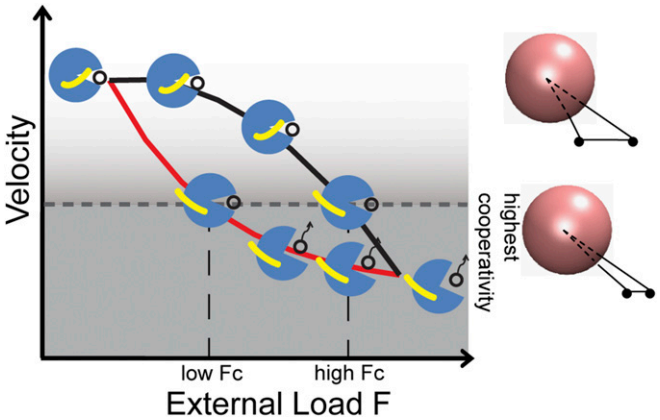

Fig. 5. A schematic force–velocity diagram with cartoons showing the spatial arrangement between the neck linker (yellow) and the motor head of a leading kinesin (blue spheres). The black open circles represent ATP. The upper black curve denotes the motion of a WT kinesin with a neck linker that detaches from the motor head at a force close to the stall force. The lower red curve denotes the motion of a kinesin mutant with a neck linker that detaches from the motor head at a force much lower than the stall force. F_c is the total force on the two interacting kinesins in a triangular configuration when the two are at the smallest separation on an MT, reaching a possibly highest cooperativity. Two WT kinesins reach this highest cooperativity at a higher external load than the two mutants.

Methods

We used the C_α-only structure-based model (44) to represent two sets of coarse-grained models, a single load-bearing motor and two load-bearing motors. The system of the singe load-bearing motor includes a 16-nm MT and a single double-headed kinesin that carries a cargo. This kinesin binds to the MT on the surface (as shown in Fig. S7*A*). The system of the two load-bearing motors includes two 16-nm MTs and two double-headed kinesins that jointly carry a cargo. Each kinesin binds to an MT on the surface (as shown in Fig. 3*A*). The Hamiltonian of the system follows a previous work (45) with several modifications. The details of the Hamiltonian can be found in *Coarse-Grained Model and Hamiltonian*. The model was created by using the web server SMOG (46).

We used the Langevin equations of motion for the coarse-grained molecular simulations. An in-house version of Gromacs4.5 (47, 48) was developed, where the nonbonded interactions were represented by a Gaussian formula. The Langevin equations of motion were integrated in the low friction limit with a damping coefficient of 1.0 τ_L^{-1} (49). The integration time step is $10^{-3}\tau_L$, where $\tau_L = (m\sigma^2/\varepsilon)^{0.5}$; m is the mass of a C_α bead, ε is the solvent-mediated interaction, and σ is the van der Waals radius of a C_α bead. We collected over 50,000 statistically significant conformations for data convergence. Thermodynamic properties and errors from the samples were computed with the weighted histogram analysis method (50).

ACKNOWLEDGMENTS. Work at the Center for Theoretical Biological Physics was sponsored by National Science Foundation Grant PHY-1427654.

1. Hancock WO (2014) Bidirectional cargo transport: Moving beyond tug of war. *Nat Rev Mol Cell Biol* 15:615–628.
2. Welte MA (2004) Bidirectional transport along microtubules. *Curr Biol* 14:R525–R537.
3. Kozielski F, et al. (1997) The crystal structure of dimeric kinesin and implications for microtubule-dependent motility. *Cell* 91:985–994.
4. Shang Z, et al. (2014) High-resolution structures of kinesin on microtubules provide a basis for nucleotide-gated force-generation. *Elife* 3:e04686.
5. Chuang TW, Chang WL, Lee KM, Tarn WY (2013) The RNA-binding protein Y14 inhibits mRNA decapping and modulates processing body formation. *Mol Biol Cell* 24:1–13.
6. Sablin EP, Kull FJ, Cooke R, Vale RD, Fletterick RJ (1996) Crystal structure of the motor domain of the kinesin-related motor ncd. *Nature* 380:555–559.
7. Carter AP, Cho C, Jin L, Vale RD (2011) Crystal structure of the dynein motor domain. *Science* 331:1159–1165.
8. Kon T, et al. (2012) The 2.8 Å crystal structure of the dynein motor domain. *Nature* 484:345–350.
9. Rayment I, et al. (1993) Three-dimensional structure of myosin subfragment-1: A molecular motor. *Science* 261:50–58.
10. Fisher ME, Kolomeisky AB (2001) Simple mechanochemistry describes the dynamics of kinesin molecules. *Proc Natl Acad Sci USA* 98:7748–7753.
11. Mandelkow E, Johnson KA (1998) The structural and mechanochemical cycle of kinesin. *Trends Biochem Sci* 23:429–433.
12. Roberts AJ, Kon T, Knight PJ, Sutoh K, Burgess SA (2013) Functions and mechanics of dynein motor proteins. *Nat Rev Mol Cell Biol* 14:713–726.
13. Hyeon C, Onuchic JN (2007) Internal strain regulates the nucleotide binding site of the kinesin leading head. *Proc Natl Acad Sci USA* 104:2175–2180.
14. Verhey KJ, Hammond JW (2009) Traffic control: Regulation of kinesin motors. *Nat Rev Mol Cell Biol* 10:765–777.
15. Vallee RB, McKenney RJ, Ori-McKenney KM (2012) Multiple modes of cytoplasmic dynein regulation. *Nat Cell Biol* 14:224–230.
16. Porter ME (1996) Axonemal dyneins: Assembly, organization, and regulation. *Curr Opin Cell Biol* 8:10–17.
17. Bresnick AR (1999) Molecular mechanisms of nonmuscle myosin-II regulation. *Curr Opin Cell Biol* 11:26–33.
18. Ito M, Nakano T, Erdodi F, Hartshorne DJ (2004) Myosin phosphatase: Structure, regulation and function. *Mol Cell Biochem* 259:197–209.
19. Hyeon C, Onuchic JN (2007) Mechanical control of the directional stepping dynamics of the kinesin motor. *Proc Natl Acad Sci USA* 104:17382–17387.
20. Shastry S, Hancock WO (2010) Neck linker length determines the degree of processivity in kinesin-1 and kinesin-2 motors. *Curr Biol* 20:939–943.
21. Wang S, Wolynes PG (2012) Active contractility in actomyosin networks. *Proc Natl Acad Sci USA* 109:6446–6451.
22. Jamison DK, Driver JW, Rogers AR, Constantinou PE, Diehl MR (2010) Two kinesins transport cargo primarily via the action of one motor: Implications for intracellular transport. *Biophys J* 99:2967–2977.
23. Driver JW, et al. (2011) Productive cooperation among processive motors depends inversely on their mechanochemical efficiency. *Biophys J* 101:386–395.
24. Uppulury K, et al. (2013) Analysis of cooperative behavior in multiple kinesins motor protein transport by varying structural and chemical properties. *Cell Mol Bioeng* 6:38–47.
25. Visscher K, Schnitzer MJ, Block SM (1999) Single kinesin molecules studied with a molecular force clamp. *Nature* 400:184–189.
26. Sugi H, Chaen S (2003) Force-velocity relationships in actin-myosin interactions causing cytoplasmic streaming in algal cells. *J Exp Biol* 206:1971–1976.
27. Belyy V, Hendel NL, Chien A, Yildiz A (2014) Cytoplasmic dynein transports cargos via load-sharing between the heads. *Nat Commun* 5:5544.
28. Bryngelson JD, Wolynes PG (1989) Intermediates and barrier crossing in a random energy-model (with applications to protein folding). *J Phys Chem* 93:6902–6915.
29. Carter NJ, Cross RA (2005) Mechanics of the kinesin step. *Nature* 435:308–312.
30. Coppin CM, Pierce DW, Hsu L, Vale RD (1997) The load dependence of kinesin's mechanical cycle. *Proc Natl Acad Sci USA* 94:8539–8544.
31. Rice S, et al. (1999) A structural change in the kinesin motor protein that drives motility. *Nature* 402:778–784.
32. Hahlen K, et al. (2006) Feedback of the kinesin-1 neck-linker position on the catalytic site. *J Biol Chem* 281:18868–18877.
33. Scarabelli G, Grant BJ (2013) Mapping the structural and dynamical features of kinesin motor domains. *PLOS Comput Biol* 9:e1003329.
34. Morcos F, et al. (2011) Direct-coupling analysis of residue coevolution captures native contacts across many protein families. *Proc Natl Acad Sci USA* 108:E1293–E1301.
35. Uemura S, Ishiwata S (2003) Loading direction regulates the affinity of ADP for kinesin. *Nat Struct Biol* 10:308–311.
36. Schnitzer MJ, Visscher K, Block SM (2000) Force production by single kinesin motors. *Nat Cell Biol* 2:718–723.
37. Klumpp S, Lipowsky R (2005) Cooperative cargo transport by several molecular motors. *Proc Natl Acad Sci USA* 102:17284–17289.
38. Müller MJI, Klumpp S, Lipowsky R (2008) Tug-of-war as a cooperative mechanism for bidirectional cargo transport by molecular motors. *Proc Natl Acad Sci USA* 105:4609–4614.
39. Kunwar A, Vershinin M, Xu J, Gross SP (2008) Stepping, strain gating, and an unexpected force-velocity curve for multiple-motor-based transport. *Curr Biol* 18:1173–1183.
40. Lu H, et al. (2012) Collective dynamics of elastically coupled myosin V motors. *J Biol Chem* 287:27753–27761.
41. Pilling AD, Horiuchi D, Lively CM, Saxton WM (2006) Kinesin-1 and Dynein are the primary motors for fast transport of mitochondria in Drosophila motor axons. *Mol Biol Cell* 17:2057–2068.
42. Saxton WM, Hollenbeck PJ (2012) The axonal transport of mitochondria. *J Cell Sci* 125:2095–2104.
43. Soppina V, Rai AK, Ramaiya AJ, Barak P, Mallik R (2009) Tug-of-war between dissimilar teams of microtubule motors regulates transport and fission of endosomes. *Proc Natl Acad Sci USA* 106:19381–19386.
44. Clementi C, Nymeyer H, Onuchic JN (2000) Topological and energetic factors: What determines the structural details of the transition state ensemble and "en-route" intermediates for protein folding? An investigation for small globular proteins. *J Mol Biol* 298:937–953.
45. Zhang Z, Thirumalai D (2012) Dissecting the kinematics of the kinesin step. *Structure* 20:628–640.
46. Noel JK, Whitford PC, Sanbonmatsu KY, Onuchic JN (2010) SMOG@ctbp: Simplified deployment of structure-based models in GROMACS. *Nucleic Acids Res* 38:W657–W661.
47. Van Der Spoel D, et al. (2005) GROMACS: Fast, flexible, and free. *J Comput Chem* 26:1701–1718.
48. Lammert H, Schug A, Onuchic JN (2009) Robustness and generalization of structure-based models for protein folding and function. *Proteins* 77:881–891.
49. Veitshans T, Klimov D, Thirumalai D (1997) Protein folding kinetics: Timescales, pathways and energy landscapes in terms of sequence-dependent properties. *Fold Des* 2:1–22.
50. Hub JS, de Groot BL, van der Spoel D (2010) g_wham-A free weighted histogram analysis implementation including robust error and autocorrelation estimates. *J Chem Theory Comput* 6:3713–3720.
51. Ogden RW, Saccomandi G, Sgura I (2007) Computational aspects of Worm-Like-Chain interpolation formulas. *Comput Math Appl* 53:276–286.
52. Noel JK, Whitford PC, Onuchic JN (2012) The shadow map: A general contact definition for capturing the dynamics of biomolecular folding and function. *J Phys Chem B* 116:8692–8702.
53. Weinkam P, Zong C, Wolynes PG (2005) A funneled energy landscape for cytochrome c directly predicts the sequential folding route inferred from hydrogen exchange experiments. *Proc Natl Acad Sci USA* 102:12401–12406.
54. Christiansen A, Wang Q, Samiotakis A, Cheung MS, Wittung-Stafshede P (2010) Factors defining effects of macromolecular crowding on protein stability: An in vitro/in silico case study using cytochrome c. *Biochemistry* 49:6519–6530.
55. Hyeon C, Klumpp S, Onuchic JN (2009) Kinesin's backsteps under mechanical load. *Phys Chem Phys* 11:4899–4910.